Biomaterials Science

ROYAL SOCIETY OF CHEMISTRY

PAPER

View Article Online
View Journal | View Issue

Cite this: *Biomater. Sci.*, 2024, **12**, 468

Fibrous capsule-resistant, controllably degradable and functionalizable zwitterion-albumin hybrid hydrogels†

Zuolong Liu,‡[a] Xianchi Zhou,‡[a] Yongcheng Chen,[a] Yanwen Ni,[a] Zihao Zhu,[a] Wenzhong Cao,[a] Kexin Chen,[a] Yu Yan,[a] Jian Ji [a,b] and Peng Zhang *[a,b]

Received 1st November 2023,
Accepted 26th November 2023

DOI: 10.1039/d3bm01783d

rsc.li/biomaterials-science

Foreign body response (FBR) represents an immune-mediated cascade reaction capable of inducing the rejection of foreign implants, thereby compromising their *in vivo* performance. Pure zwitterionic hydrogels have demonstrated the ability to resist long-term FBR, owing to their outstanding antifouling capabilities. However, achieving such a robust anti-FBR effect necessitates stringent requirements concerning the purity of zwitterionic materials, which constrains their broader functional applications. Herein, we present a biocompatible, controllably degradable, and functionalizable zwitterion-albumin hybrid hydrogel. The zwitterionic hydrogel crosslinked with serum albumin exhibits controllable degradation and excels in preventing the adsorption of various proteins and adhesion of cells and bacteria. Moreover, the hydrogel significantly alleviates the host's FBR compared with PEG hydrogels and particularly outperforms PEG-based cross-linker crosslinked zwitterionic hydrogels in reducing collagen encapsulation when subcutaneously implanted into mice. The zwitterion-albumin hybrid hydrogel shows potential as a functionalizable anti-FBR material in the context of implantable materials and biomedical devices.

1. Introduction

Implantable biomaterials can trigger host recognition, initiating a cascade of immune-mediated foreign body responses (FBRs).[1–6] This cascade involves the infiltration of immune cells, intense inflammatory responses, fibrosis, and subsequent dense fibrous capsule formation.[7–10] These developments eventually isolate the implants from the host, significantly impairing the functionality of biomaterials and the signal fidelity of implanted biomedical devices.[11–18]

Over the past decade, significant advances have been made in the development of anti-fibrotic materials.[19–25] For example, pure zwitterionic hydrogels have demonstrated their ability to resist capsule formation for up to 1 year in rodent models.[23,24] As a unique type of material, zwitterionic polymers bear a pair of oppositely charged groups in their repeating units, which exhibit an overall neutral charge with a strong hydration effect *via* ionic solvation.[26] Consequently, zwitterionic materials are capable of resisting non-specific protein adsorption on the material surface, a crucial step in the initiation of the FBR process.[27] However, the remarkable FBR resistance observed in zwitterionic hydrogels is based on their high zwitterionic purity. Previous studies have shown that zwitterionic hydrogels copolymerized with 2-hydroxyethyl methacrylate (HEMA) or PEG showed similar or even stronger capsule formation than PHEMA and PEG hydrogels in implantation experiments.[28,29] The aforementioned findings underscore the critical importance of zwitterionic hydrogel purity in achieving effective anti-FBR performance, which excludes the possibility of functionalizing those anti-FBR zwitterionic hydrogels. In addition, on-demand degradation of capsule-resistant zwitterionic hydrogels is often needed for temporary implants.[30]

In this work, we report a zwitterion-albumin hybrid hydrogel consisting of poly(carboxybetaine) (PCB) and serum albumin. Albumin is the most abundant plasma protein in the human blood, which is widely applied in clinical settings due to its well-established biological safety and remarkable functional versatility.[31–33] Similar to many bioinert protein structures, it has been shown to be low immunogenic and resistant to long-term inflammatory responses.[34–36] Material surfaces coated with serum albumin showed significantly improved biocompatibility for implantation.[37,38] In addition, serum albumin exhibits the capacity to bind to a wide range of

[a]*MOE Key Laboratory of Macromolecule Synthesis and Functionalization, Department of Polymer Science and Engineering, Zhejiang University, Hangzhou, P. R. China. E-mail: zhangp7@zju.edu.cn*
[b]*International Research Center for X Polymers, International Campus, Zhejiang University, Haining, P. R. China*

†Electronic supplementary information (ESI) available. See DOI: https://doi.org/10.1039/d3bm01783d

‡These authors contributed equally.

different endogenous and exogenous compounds through hydrophobic interactions within the cavity, making it a widely employed carrier for drug loading and a scaffold material for the transport and controlled release of bioactive molecules.[39–42] Considering the aforementioned advantages of albumin, we hypothesize that the incorporation of serum albumin into zwitterionic hydrogels may endow the material with controllable biodegradability and functionalizability, without compromising its fibrotic capsule resistance. The hybrid hydrogel was synthesized by copolymerization of carboxybetaine monomers with surface acrylated human serum albumin. This integration effectively preserves ultra-low biofouling and anti-FBR performance while introducing the potential for further functionalization. In addition, the biodegradation of the hybrid hydrogel can be easily controlled by the degree of albumin acylation. Moreover, the hydrogel induced minimal inflammation and effectively mitigated the FBR in murine models for 3 months.

2. Experimental

2.1 Materials

Human serum albumin was obtained from the FEIYUBIO biotech company. 2-((2-Acrylamidoethyl)dimethyl ammonio) acetate (CBAA-2) was synthesized following previous reports.[43] Poly(ethylene glycol)diacrylate (PEGDA; M_n 2000), 4-arm poly (ethylene glycol)acrylate (4-arm PEG-AC; M_n 10 000), *N*-acryloxysuccinimide (NAS), ammonium persulfate (APS), *N*,*N*,*N*′,*N*′-tetramethylethylenediamine (TEMED; 99%), tris(2-carboxyethyl)phosphine (TCEP), picrylsulfonic acid solution (TNBS; 5% in water), fibrinogen from human plasma (≥80% clottable protein), phosphate-buffered saline [PBS, 1 mM (pH 7.4)] and fibrinogen from human plasma (≥80% clottable protein) were purchased from Sigma-Aldrich.

2.2 Protein modification

Human serum albumin (HSA) was first modified to introduce an acryloyl group onto its surface. The reaction was performed by dissolving 200 mg of HSA in 10 mL of 50 mM Hepes buffer (pH 8.5), followed by dropwise addition of 500 μL or another volume of NAS dimethyl sulfoxide (DMSO) solution (20 mg mL^{-1}). The reaction mixture was slowly stirred at 4 °C for 2 h. The reaction mixture was concentrated and washed extensively with PBS 7.4 using 10 kDa molecular weight cutoff centrifugal filters. The albumin solution was preserved at a temperature of 4 °C for use with a concentration of 20 mg mL^{-1} finally.

2.3 Preparation of the hydrogel

The reactant solutions were prepared with 0.01M phosphate buffer solution (PBS). Most of the hybrid hydrogels were prepared following a one-step sequential free-radical polymerization method. In general, the CBAA monomer at a constant amount of 20% (mass percent of solution) was added to a precursor solution of the modified protein. Then 4 ‰ (wt/vol) of the initiator APS and the catalyst TEMED were added into the solution and dispersed by gentle shaking. The mixture was quickly transfused in the prepared sheet mold separated by 1 mm polytetrafluoroethylene (PTFE) or a tubular rod mold. The mold loaded with the resulting solution was reacted in a room environment for 1 hour. The hydrogels were removed from the slides and equilibrated in a PBS buffer for 3 days. The PBS buffer was changed three times daily to remove unreacted chemicals. Biopsy punches were used to punch hydrogels into 5 mm-diameter disks. For comparison, PEG hydrogels and PCB hydrogels using PEGDA as the crosslinker were prepared for performance contrast.

2.4 Mechanical properties and water content tests

To test the mechanical strength of hydrogels, at least five 10 mm diameter disks of each formulation (5 mm thickness when cast), which were allowed to reach swelling equilibrium in PBS, were compressed to failure at a rate of 1 mm min^{-1} using a mechanical tester with a 20 kN load cell. The Young's modulus was calculated from 3 to 13% strain to avoid any complications in the instance where the top platen might not be completely engaged with the specimen when compression begins. Similarly, 5 mm diameter and 1 mm height disks were used to test their surface mechanical properties using a Nanoindenter after swelling sufficiently.

The equilibrium water contents (EWCs) of equilibrated hydrogels were measured through a gravimetric method. Hydrogel disks (5 mm in diameter and 1 mm in thickness) were allowed to swell in PBS until reaching equilibrium at 37 °C. The equilibrated samples were taken out, and their wet masses (M_w) were measured after the removal of excess water on the surface by rolling them on filter paper. The samples were then snap-frozen in liquid nitrogen and lyophilized for 2 days until complete dryness is achieved and their dry masses (M_d) were measured. The EWCs were calculated as follows:

$$\mathrm{EWC} = \frac{M_w - M_d}{M_w} \times 100\%$$

2.5 Biodegradability test of hydrogels *in vitro*

In the preparation of the hydrogel, zwitterion monomers were added to the albumin crosslinking agent solution, 0.4% Trypan Blue stain was added at the same time and incubated for 15 min to label the zwitterion, and then the initiator and catalyst were added for subsequent polymerization to form the hydrogel as described above. The prepared zwitterion/albumin hydrogels with at least 5 mm thickness and 10 mm height were incubated in 10 ml of 0.25% trypsin-EDTA buffer at room temperature with PBS (pH = 7.4) as the control. At regular intervals, 100 μl of trypsin enzyme solution and the substrate solution of the control group after incubation for different times were collected, and their absorption intensity at 525 nm was tested with a plate reader, which was recorded as Ab_{enz} and Ab_{pbs} respectively, and the absorbance of the substrate solution after complete degradation of the hydrogel was recorded as Ab_{compl}. At this time, the absorbance of the hydrogel substrate solution in the control group was expressed as

Ab_{con}. Then the degradation degree of the albumin hydrogel could be calculated using the following formula:

$$\text{Degradation Rate} = \frac{Ab_{enz} - Ab_{pbs}}{Ab_{compl} - Ab_{con}} \times 100\%$$

2.6 Biodegradability test of hydrogels *in vivo*

All animal procedures were performed in accordance with the Guidelines for Care and Use of Laboratory Animals of Zhejiang University and approved by the Animal Ethics Committee of Zhejiang University. Healthy male BALB/c nude mice (4–5 weeks old, weighing around 16 g) were purchased from the animal center of Zhejiang Academy of Medical Sciences. The mice subcutaneous implantation model was adopted. Hydrogel disks were implanted subcutaneously into the dorsal pockets of male mice by making a subcutaneous incision along the centerline of the back shoulder blades. Each animal received six implants, and each implant consisted of unique hydrogel chemistry. After the hydrogel discs were implanted into the back of mice, the mice were sacrificed at 2 weeks, 1 month, and 3 months after implantation, respectively. The backs of the mice were dissected to observe the shape changes of the implanted materials in the mice, and the changes in the area of the implanted hydrogel were counted, which indirectly characterized the degradation of the gel *in vivo*.

2.7 Cell adhesion

Human umbilical vein epithelial cells were selected for the cell adhesion assay of the hydrogels. Hydrogel disks of 5 mm diameter were placed in individual wells in a 48-well plate with 500 μL of PBS solution in each well. To sterilize the hydrogels, they were irradiated with UV light for 30 min and refrigerated overnight in penicillin–streptomycin in PBS. Human umbilical vein epithelial cells (p = 6) were seeded onto the hydrogels at a concentration of 10^5 cells per ml in a supplemented Roswell Park Memorial Institute-1640 (RPMI-1640) medium. Cells were allowed to grow for 8 h at 37 °C, 5% CO_2, and 100% humidity. The medium was then removed, and the hydrogels were gently washed with PBS. For fluorescent imaging, the cells were stained with SYTO9 following the manufacturer's protocol and then observed under a fluorescence microscope. Absorbance was normalized using cells cultured on the TCPS sample as 100%. Average data were acquired from six specimens.

2.8 Bacterial adhesion

Microbial adhesion assay was performed using a previously reported method with modifications. Gram positive bacteria *Staphylococcus aureus* (ATCC 6538) and Gram negative bacteria *Pseudomonas aeruginosa* (ATCC 15442) were used. Bacteria were cultured in a Luria Bertani (LB) medium. The bacteria were incubated in the medium with 200 rpm shaking and cultured respectively to reach the exponential growth stage. When the suspension culture reached a light absorption intensity of 1.0 at 600 nm, the bacteria were centrifuged at 5000 rpm and re-suspended in sterile PBS at a concentration of 10^8 CFU mL^{-1}. The microorganisms were stained with SYTO9 (Invitrogen, S34854) for 20 min, centrifuged and re-suspended to the original volume, then added to different hydrogel discs in the holes or empty holes, and cultured at 37 °C for 8 h. Subsequently, the holes were gently washed with sterile PBS to remove non-adherent bacteria and the results were directly observed using a fluorescence microscope.

2.9 Hydrogel implanting subcutaneously in mice

All animal procedures were performed in accordance with the Guidelines for Care and Use of Laboratory Animals of Zhejiang University and approved by the Animal Ethics Committee of Zhejiang University. Healthy male BALB/c nude mice (4–5 weeks old, weighing around 16 g) were purchased from the animal center of Zhejiang Academy of Medical Sciences. Mice were raised in an IVC system at 20–26 °C and 40–70% humidity, with a dark/light cycle of 12 h. All hydrogels were tested for endotoxin using a Limulus Amebocyte Lysate (LAL) endotoxin assay kit (Solarbio, catalog no. T7574) prior to implantation. The hydrogel had been proved to have negligible endotoxin. Hydrogel samples were swollen with sterile PBS, sterilized by UV and implanted subcutaneously into C57BL/6 male mice at 6-week-old. Five replicates for each type of hydrogel were implanted into mice. Mice were anesthetized using pentobarbital and shaved. About an 8 mm longitudinal incision was made on the dorsal surface, using surgical scissors, to provide access to the subcutaneous space. Then subcutaneous pockets on either side of the incision were created with blunt forceps for the implantation of the hydrogel disks. After implantation, the incisions were closed using medical surgical sutures. Mice were monitored until recovery from anesthesia and housed for 2 weeks, 4 weeks, and 3 months. The mice grew normally with no sign of discomfort after the implantation and no loss in body weight was observed before explantation compared with the control group. After each time point, mice were sacrificed and the hydrogel samples together with the surrounding tissues were excised and collected. The explanted samples were fixed in 4% paraformaldehyde overnight and embedded in paraffin wax. Sections of each sample at 3–5 μm thickness were cut and mounted onto slides for histological staining and imaging. All images were scanned with Pannoramic 250/MIDI-equipped with the CaseViewer 2.0 software. All data are presented as a mean of biological replicates.

2.10 Histological analysis

The chronic inflammatory response was examined by staining the tissue sections 1 month and 3 months post implantation with hematoxylin & eosin (H&E), which stains nuclei in blue and cell cytoplasm in pink. Collagen formation and distribution were examined by staining the tissue sections 4 weeks and 3 months post implantation with Masson's trichrome (M&T) that stains collagen in blue, cytoplasm in red, and nuclei in black. The inflammatory cell thickness is measured according to the thickness of the markedly red to purple layer at the hydrogel–tissue interface in the M&T images (n = 6, mean values ± s.d.). The collagen density is measured by the percentage of blue-pixel coverage in the M&T images of tissues

within 50 μm (at 10 μm steps) from the hydrogel–tissue interface. The collagen densities and thickness of the subcutaneous skin tissues from different mice were analyzed using the corresponding Masson's trichrome staining histological images (as described above) *via* the ImageJ software.

2.11 Macrophage immunofluorescence

Before the immunofluorescence assay, antigen retrieval, fluorescence cancellation, and serum blocking were performed. To stain macrophages after 2 weeks of implantation, sections were incubated with a rabbit anti-mouse F4/80 monoclonal antibody (dilution 1 : 400; catalog no. 30325 from Cell Signaling Technology) overnight at 4 °C. After being washed three times with phosphate-buffered saline (PBS), the sections were incubated with an Alexa Fluor® 488-conjugated goat anti-rabbit IgG (H + L) antibody (dilution 1 : 400; catalog no. GB25303 from Servicebio) for 50 min in the dark. The sections were washed three times with PBS and incubated with DAPI (1 μg mL^{-1} in PBS) for 10 min. The macrophages show green fluorescence and the nucleus shows blue fluorescence.

2.12 Immunohistochemical staining of inflammatory factors

Acute inflammation of the implant can be characterized by this method. The rabbit anti-mouse CCR-7 monoclonal antibody is from Novus Biologicals (dilution 1 : 200; catalog no. NBP2-67324). The rabbit anti-mouse TNF-α polyclonal antibody is from Servicebio (dilution 1 : 400; catalog no. GB11188). The goat anti-mouse IL-6 polyclonal antibody is from Novus Biologicals (dilution 1 : 100; catalog no. NB600-1443). The goat anti-mouse IL-17 polyclonal antibody is from Novus Biologicals (dilution 1 : 100; catalog no. AF519). Before immunoassay, antigen retrieval, endogenous peroxidase cancellation, and bovine serum albumin blocking were performed sequentially. Sections of samples 2 weeks post-implantation were incubated with a primary antibody overnight at 4 °C. The sections were washed three times with PBS and incubated with a HRP-labeled goat anti-rabbit antibody or a HRP-labeled rabbit anti-goat antibody (1 : 200; catalog no. GB23303 or GB23204 from Servicebio) at room temperature for 50 min in the dark. Sections were washed three times, dried slightly, and then incubated with a freshly prepared diaminobenzidine (DAB) chromogenic reagent kit (DAKO, catalog no. K5007). The sections were counterstained for the nucleus with a Hematoxylin staining solution (Servicebio, catalog no. G1004) for 3 min and washed with water. Cells stained by inflammatory markers show a brown color, while all nuclei stained with hematoxylin show blue color. The degree of positive expressions around each hydrogel (within 100 μm from the hydrogel–tissue interface) was measured (n = 6, mean values ± s.d.).

2.13 Data analysis

All examination and quantitative results were obtained for at least five samples for analysis. The histological sections were observed with at least five random images in each section on two sections per animal. Results are expressed as the means of at least five replicates and SD (standard deviation). All data are expressed and presented as means and SD. Statistical analyses were performed with Origin 2023 and GraphPad Prism 9 software.

3. Results and discussion

3.1 Material preparation and characterization

We used a straightforward approach to introduce multiple double bonds onto human serum albumin (HSA), creating an albumin-based cross-linker termed ALB-Ac as depicted in Fig. 1a. The lysine residues on the albumin surface were utilized as sites for modification. The extent of double bond modification on the protein was controllable by introducing varying quantities of *N*-acryloxysuccinimide to a specified concentration of HSA, labeled as H20, H10 and H5 (Table S1 and S2†). Using the TNBS reagent, we quantitatively measured the amine content, allowing us to calculate the degree of double bond grafting on the protein surface.[44] As shown in Table S1,† about 81%, 58% and 29% of the primary amines on the albumin surface were successfully acrylated for H20, H10 and H5, respectively. Next, we prepared a series of PCB-HSA hydrogels by free radical polymerization with a constant protein content of ~10% of the total solid. To study whether the protein folding structure affects the performance, we also prepared a sample with de-folded HSA (PCB-H20S). PEG hydrogels and PCB-PEG hydrogels were also prepared as the controls.

It is widely acknowledged that material modulus significantly affects the extent of fibrosis induced by the implants.[45–47] Before the *in vivo* test, we compared the mechanical properties of the hydrogels. As shown in Fig. 1b, the prepared PEG, PCB-PEG, PCB-H20S and PCB-H20 hydrogels displayed similar compressive modulus. However, due to the reduced double bond density introduced on albumin, the crosslinking densities of PCB-H10 and PCB-H5 hydrogels notably decreased, consequently weakening their mechanical properties. The surface stiffness of PCB-HSA hydrogels exhibited a similar trend (Fig. 1c). The water content values of all prepared hydrogels are shown in Fig. 1d. Due to the superhydrophilicity, the water content values of all zwitterionic hydrogels exceeded 90%; in contrast, the PEG hydrogels had a water content of ~70%.

Biofouling, including the attachment of microorganisms and the formation of biofilms, poses a significant challenge in the context of biosensors and medical devices. It can lead to complications such as haemolysis, thrombosis, immune responses, infections, and excessive tissue growth in implants.[48] Biofouling was recognized as the first step of the foreign body response. In this study, the hybrid hydrogels were exposed to a range of biological substances, including human umbilical vein epithelial cells (HUVEC) and two bacterial strains (*Staphylococcus aureus* and *Pseudomonas aeruginosa*). The PEG and PCB-PEG hydrogels were used for comparison, while tissue culture polystyrene (TCPS) served as the positive

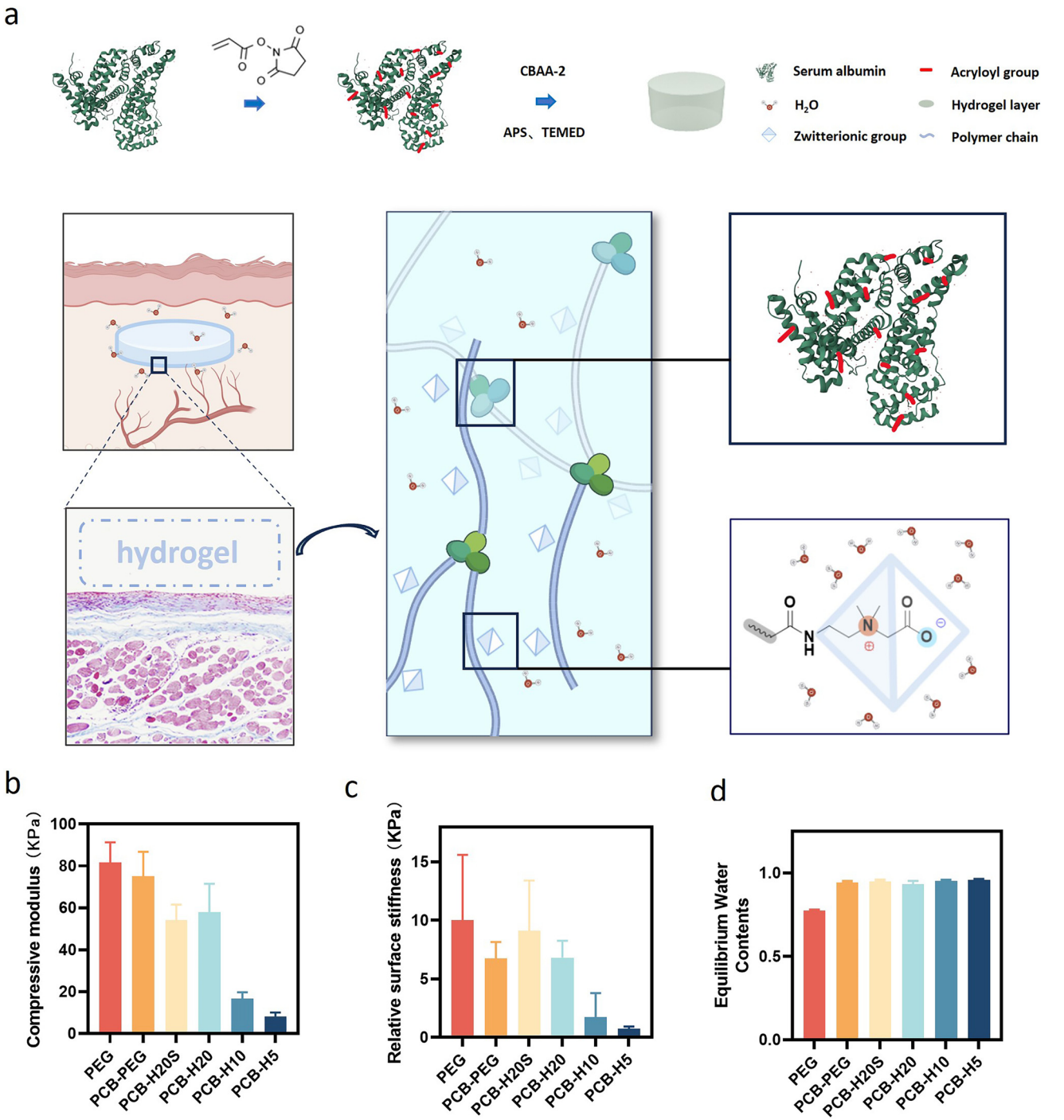

Fig. 1 The design and characterization of the hydrogels. (a) Schematic illustration of the design of the zwitterionic hybrid hydrogels. (b) Compressive modulus of the prepared hydrogels, n = 5. (c) Surface hardness of the hydrogels measured using a nano-indenter, n = 5. (d) Equilibrium water contents of the hydrogels, n = 5.

control. The results revealed that no significant adhesion of HUVEC was observed on either the PCB-PEG hydrogel or the PCB-HSA hydrogels at 8 hours post-cell seeding (Fig. 2). Although a few cells were occasionally found, they remained round in shape without signs of spreading. In contrast, a large number of cells adhered to the TCPS surface and extended thin pseudopodia, indicating spreading. Although the cell adhesion on the PEG hydrogel surface was reduced by 90% compared to the TCPS, a large number of cells were still attached to the hydrogel surface after 8 hours of culture. A Gram-positive strain of MRSA and a Gram-negative strain of *P. aeruginosa* were applied to examine the bacterial attach-

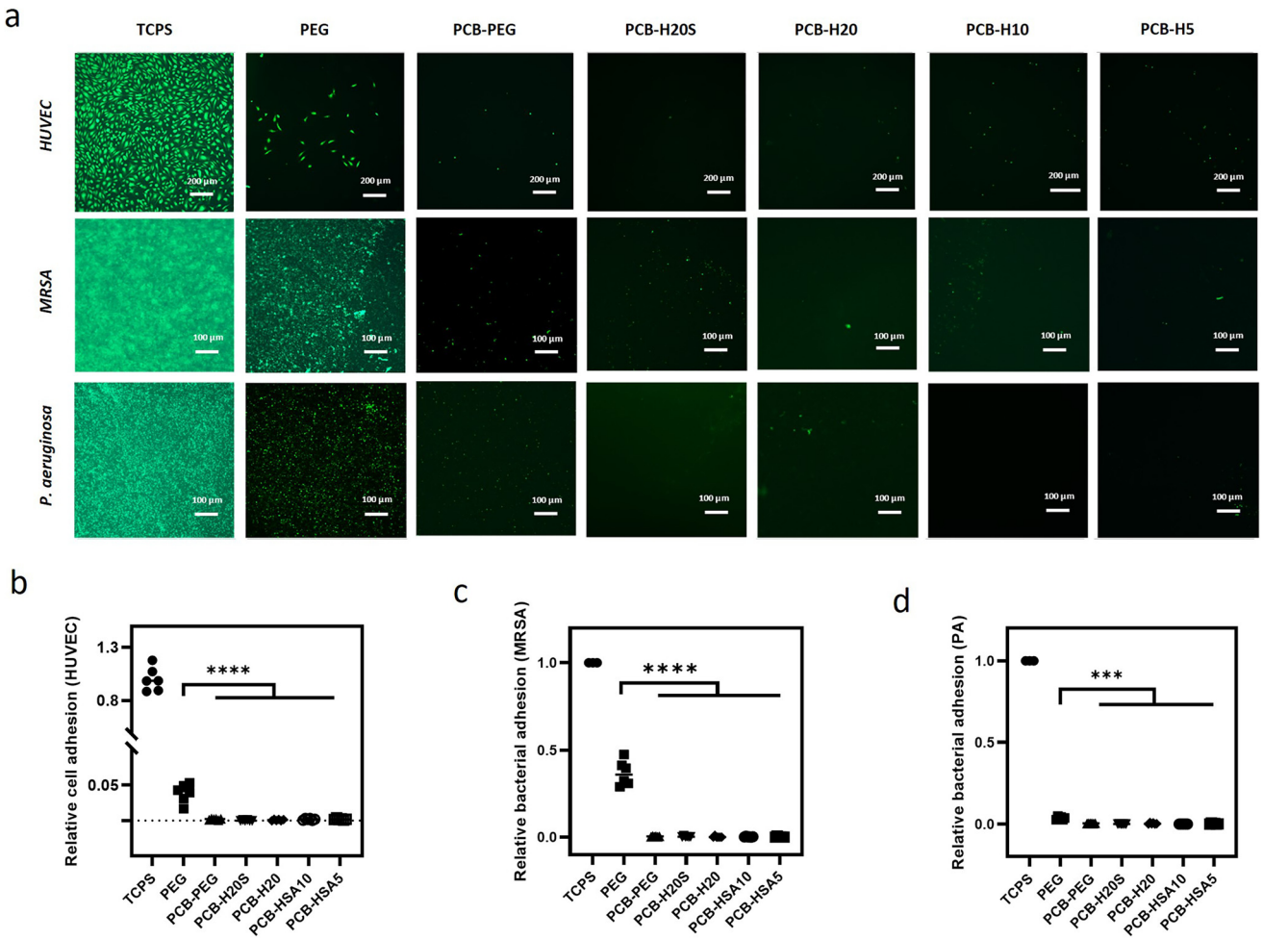

Fig. 2 Resistance of the hydrogels to endothelial cells and bacteria. (a) Fluorescence micrographs of surface attachment from cells and microbes including HUVEC, MRSA and *P. aeruginosa*. (b–d) Quantitative analysis of the surface attachment of (b) HUVEC; (c) MRSA; and (d) *P. aeruginosa* (statistical analysis: *t*-test; $n = 6$; ***$p < 0.001$; ****$p < 0.0001$).

ment, as they are the primary pathogens responsible for infections in healthcare settings and are common initial colonizers on various biomedical implants. Fluorescence image analysis revealed that PCB-HSA hydrogels and PCB-PEG hydrogels exhibited strong resistance to both types of bacteria. In contrast, substantial bacterial attachment and colonization occurred on the TCPS surfaces. PEG hydrogels also exhibited some resistance to bacterial adhesion, although the anti-adhesion effect was less pronounced. Overall, the experimental results show that copolymerization of PCB with albumin does not compromise its anti-fouling properties.

3.2 Biodegradation of the zwitterionic hybrid hydrogels

Albumin-based hydrogels are known for their excellent biocompatibility and degradability.[49] We first tested the enzymatic degradation behavior of the zwitterion–albumin hybrid hydrogels by incubating them in a trypsin solution. Trypan blue was used to label the zwitterionic hydrogels as the dye has strong bindings with the caboxybetaine groups of the hydrogel. As shown in Fig. 3c and d, all the zwitterion–albumin hybrid hydrogels degraded after a certain time of incubation. Notably, the degradation became slower with the increase of the degree of protein acrylation, as more polymer chain conjugation on the protein surface hinders the enzymatic reaction by a steric effect. In contrast, PEG and PCB-PEG exhibited minimal signs of degradation. Subsequently, we extended our investigation to explore the *in vivo* degradation behavior of the hydrogels through subcutaneous implantation in C57BL/6 mice. The *in vivo* degradation behavior was assessed by recording the sample size upon sample retrieval at various time points post-implantation (Fig. 3e). The degradation of the hydrogels was quantified by measuring the changes in the area of the remaining materials, as illustrated in Fig. 3f. It was evident that degradation occurred for all implanted zwitterion-hybrid hydrogels. The PCB-H5 sample almost completely degraded after 3-month implantation, while 40% of the PCB-H20 sample remained at the same time point. Both *in vitro* and *in vivo* degradation tests showed that the biodegradation kinetics of those hybrid hydrogels can be easily controlled by adjusting the degree of acylation of albumin.

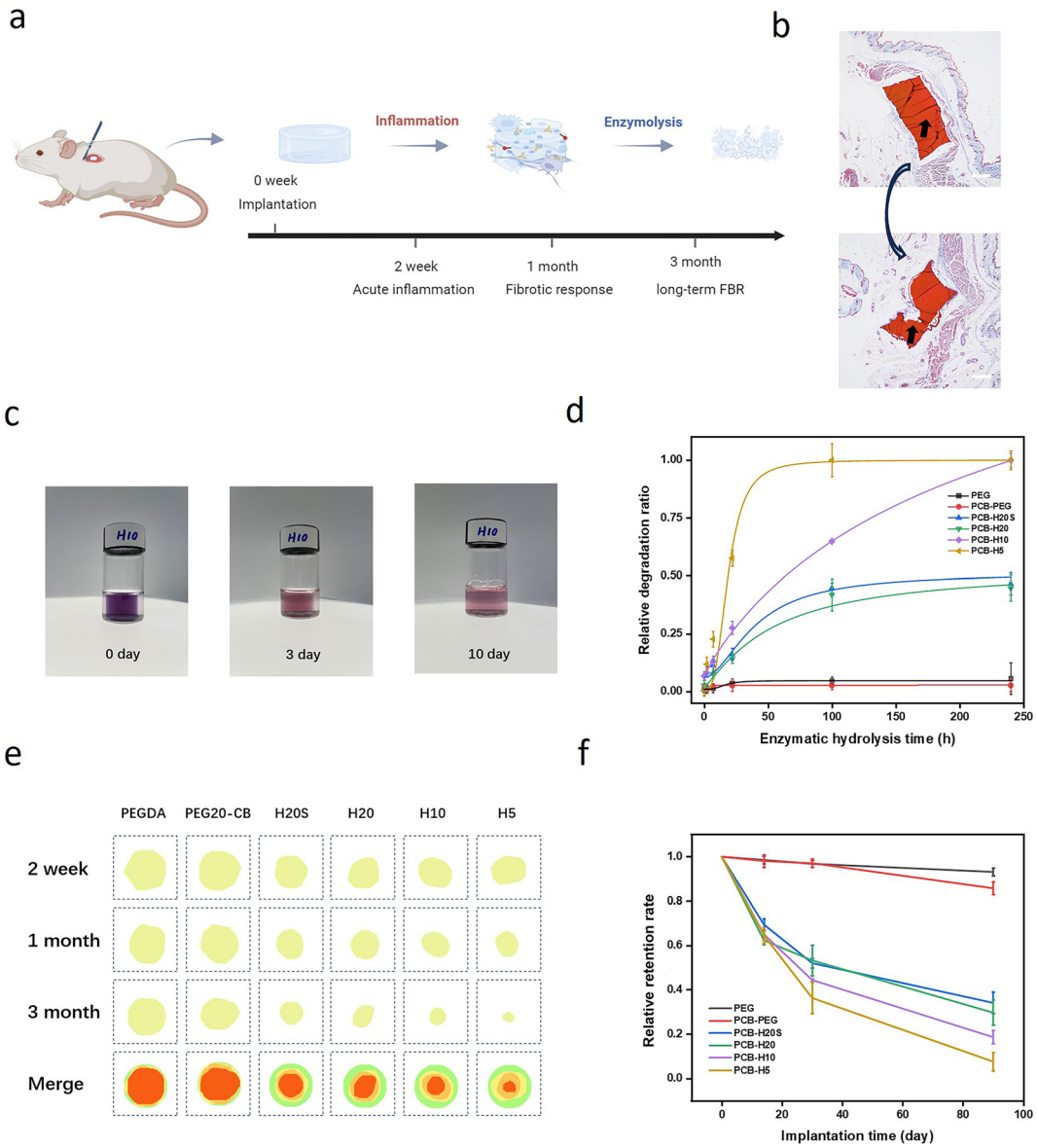

Fig. 3 Biodegradation behavior of the hydrogels *in vitro* and *in vivo*. (a) Schematic diagram of the hydrogel implantation. (b) Hydrogel morphological changes in mice after different times of subcutaneous implantation, above: 2 weeks and below: 1 month. Scale bars, 500 μm. (c) Representative images of the degradation behavior of the hydrogels in 0.25% trypsin solution. Carboxybetaine groups were labeled with Trypan blue. (d) Degradation curves of all tested hydrogels in the trypsin solution. The degree of degradation was determined by detecting the OD value of the solution at 565 nm. (e) Size and shape of the retrieved hydrogels from mice after different implantation periods. The hydrogel discs on the back of the mice were retrieved for analysis after 2 weeks, 1 month, and 3 months. (f) The area changes of the retrieved hydrogels (n = 6).

3.3 Inflammation and capsule formation after implantation

We conducted an investigation into the acute inflammatory response induced by the hybrid hydrogels following their subcutaneous implantation in C57BL/6 mice for 2 weeks, employing mice without surgery as the control group. Immunohistochemical analysis was performed to assess the impact of PCB-HSA hydrogel implantation on the level of inflammation in the neighboring tissues, focusing on pro-inflammatory markers such as CCR-7, IL-6, IL-17, and TNF-α (Fig. 4a). The results reveal a significant increase in the expression of inflammatory markers at the interface between the hydrogel and the surrounding tissue when PEG hydrogels were used. In contrast, the expression of inflammatory markers is markedly lower for PCB-HSA hydrogels. Notably, the inflammation induced by the implantation of PCB-HAS hybrid hydrogels is significantly lower than that induced by PCB-PEG hydrogels. Besides, there were no significant differences between the PCB-HSA hydrogels with different degrees of protein graft modification (Fig. 4b–d). Macrophages play a critical role in coordinating the inflammatory response and are regarded as a pivotal cell type in the traditional theory of

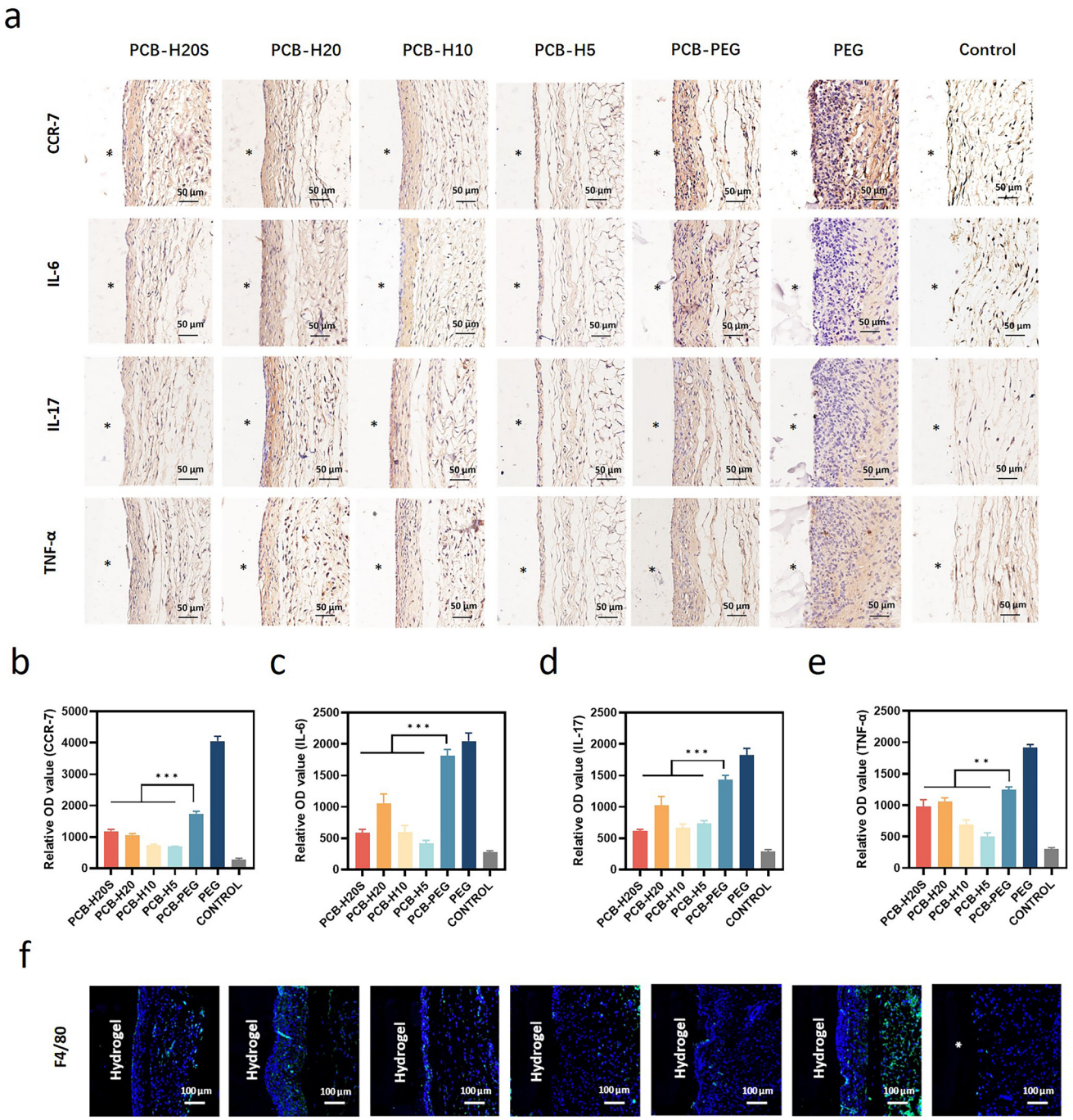

Fig. 4 Inflammation analysis 2 weeks post implantation. (a) Immunohistochemical staining of inflammatory markers (CCR7, IL-6, IL-12, and TNF-α) in tissues surrounding hydrogels. Cells stained by inflammatory markers show a brown color, while all nuclei stained with hematoxylin show blue color. Nuclei were stained with DAPI to show blue fluorescence in the middle column (* hydrogel implants). (b–e) Quantification of the inflammatory marker expression. Data were collected for the tissue within 100 μm from the tissue–hydrogel interface. (c) CCR-7; (d) IL-6; (e) IL-17; and (f) TNF-α. (f) Macrophages immunofluorescent stains. Macrophages were labeled with a pan macrophage immunofluorescent biomarker (F4/80) and were stained green (statistical analysis: *t*-test; $n = 6$; $^{**}p < 0.01$; $^{***}p < 0.001$).

FBR.[50] With this in mind, we extended our investigation to examine the impact of PCB-HSA hydrogels on macrophage behavior. Immunofluorescent staining for the F4/80 marker revealed that a substantial accumulation of macrophages occurred near PEG implants, whereas PCB-HSA implants displayed only a minimal presence of macrophages at the 2-week mark (Fig. 4f).

We further evaluated the long-term fibrotic responses of these hydrogels in a mouse model. Subcutaneous implantation tests were conducted on C57BL/6 mice, with each

mouse receiving implants of all six samples on its back. The discs were extracted at both the 1-month and 3-month time points, and representative photos and histological images are displayed in Fig. 5a. The zwitterionic hydrogels appeared red after the staining. The photos showed that hydrogels containing PEG components tended to adhere to a thick layer of surrounding tissue, whereas PCB-HSA hydrogels remained transparent, independent, and non-fouling. It can be observed that due to the degradation properties of PCB-HSA hydrogels, there were some sparsely structured areas between PCB-HSA hydrogels and tissues, displaying a very light color or transparency in the stained sections. The Masson staining results indicated that the surface of the PEG hydrogel formed a thick and dense layer of collagen within the first month. However, almost no significant blue collagen was observed around the PCB-HSA hydrogels. The collagen density at the interface of PCB-HSA hydrogels and tissues was significantly lower than that of both the PEG hydrogels and PCB-PEG hydrogels. The thickness of the collagen layer surrounding the PEG hydrogel was approximately ~40 μm, and the thickness of the PCB-PEG hydrogel was about ~30 μm. By contrast, there was almost no capsule formed around the PCB-HSA hybrid hydrogels (Fig. 5b and c). The collagen thickness and density around PCB-HSA hydrogels remained at very low levels even after 3 months of implan-

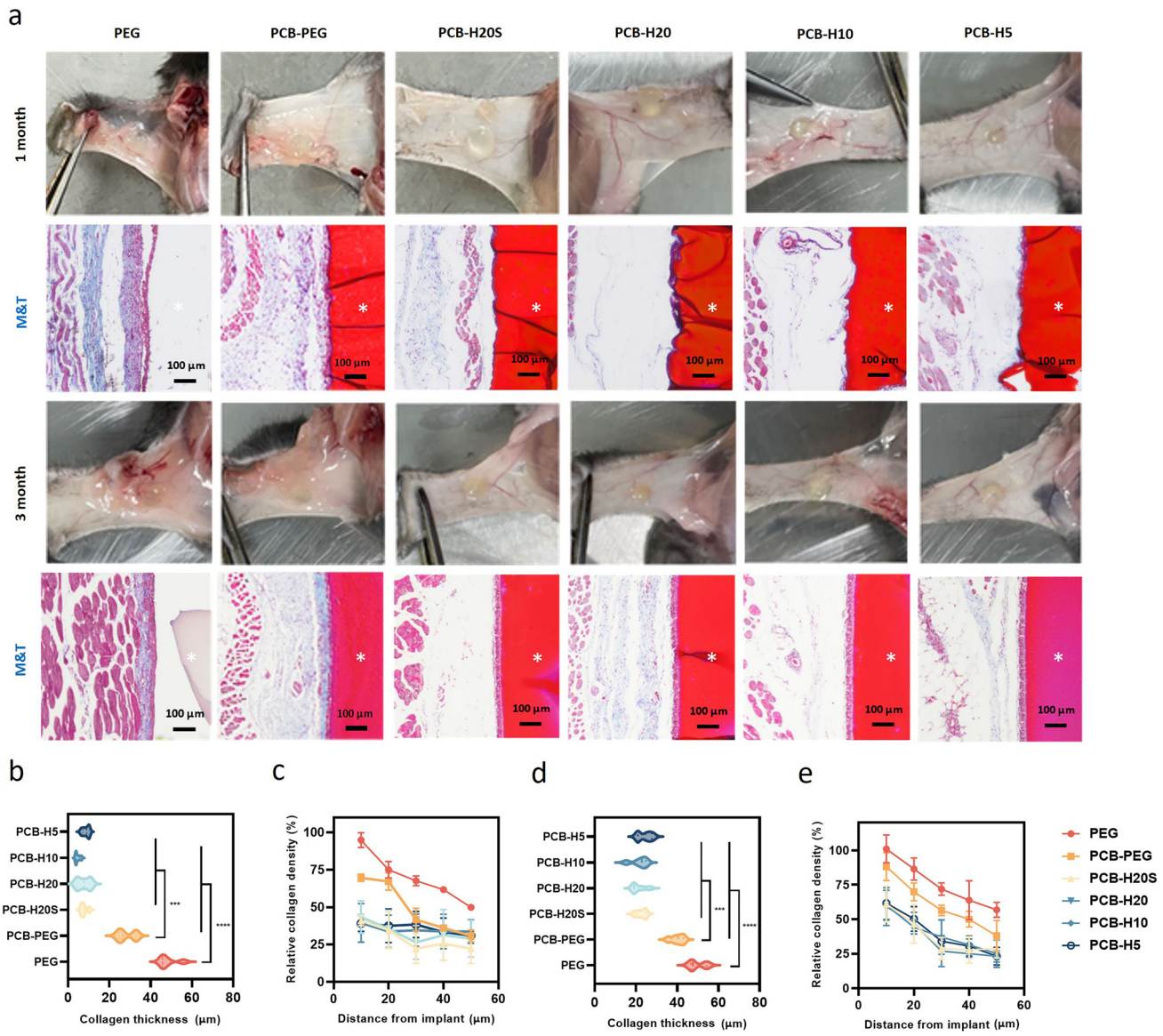

Fig. 5 Evaluation of the FBR for hydrogels implanted in mice. (a) Collagen distribution in tissues surrounding the hydrogels after 1 month and 3 months post subcutaneous implantation. M&T staining was used to evaluate the collagen encapsulation after implantation. (b–e) Statistics of collagen density and thickness at one and three months after implantation (* hydrogel implants). (b and c) Collagen thickness and density at the hydrogel–tissue interfaces after 1 month. (d and e) Collagen thickness and density at the hydrogel–tissue interfaces after 3 months (statistical analysis: *t*-test; $n = 6$; $^{**}p < 0.01$; $^{***}p < 0.001$).

tation (Fig. 5d and e), indicating that forming hybrid hydrogels with albumin does not compromise the capsule-resistance of the zwitterionic polymers. In addition, the degree of albumin acylation or the de-folding of albumin structure did not significantly affect the fibrotic response induced by hydrogel implantation.

4. Conclusion

In summary, we have synthesized a series of capsule-resistant, controllably degradable and functionalizable zwitterion-albumin hybrid hydrogels. By introducing serum albumin as a cross-linker for PCB hydrogels, we have achieved a zwitterionic hydrogel with controllable degradation and functionality. *In vitro* experiments have demonstrated that PCB-HSA hydrogels exhibited robust resistance to cell adhesion and bacterial colonization. The enzymatic degradation kinetics of the hybrid hydrogels can be fine-tuned by adjusting the degree of acylation of albumin. Upon implantation in mice, these PCB-HSA hydrogels provoked minimal inflammatory responses within 2 weeks, while also effectively inhibiting the development of collagen capsules for at least 3 months, in contrast to the strong response induced by the PCB-PEG hydrogel. The zwitterion-albumin hybrid hydrogels show potential as functionalizable anti-FBR materials for implantable materials and biomedical devices.

Conflicts of interest

There are no conflicts of interest to declare.

Acknowledgements

This work was financially supported by the National Natural Science Foundation of China (22175152 and 52103188), the Joint Funds of the Zhejiang Provincial Natural Science Foundation of China and Huadong Medicine (LHDMZ22H300011), the National Key Research and Development Program of China (2022YFB3807300), the Fundamental Research Funds for the Central Universities (226-2022-00146), and the startup package from Zhejiang University.

References

1 R. Beatty, K. L. Mendez, L. H. J. Schreiber, R. Tarpey, W. Whyte, Y. Fan, S. T. Robinson, J. O'Dwyer, A. J. Simpkin, J. Tannian, P. Dockery, E. B. Dolan, E. T. Roche and G. P. Duffy, *Sci. Robot*, 2023, **8**, eabq4821.
2 N. Kutner, K. R. Kunduru, L. Rizik and S. Farah, *Adv. Funct. Mater.*, 2021, **31**, 2010929.
3 D. Zhang, Q. Chen, C. Shi, M. Chen, K. Ma, J. Wan and R. Liu, *Adv. Funct. Mater.*, 2020, **31**, 2007226.
4 O. Veiseh and A. J. Vegas, *Adv. Drug Delivery Rev.*, 2019, **144**, 148–161.
5 J. M. Anderson, A. Rodriguez and D. T. Chang, *Semin. Immunol.*, 2008, **20**, 86–100.
6 B. Yang, N. Rutkowski and J. Elisseeff, *Biomater. Sci.*, 2023, **11**(24), 7730–7747.
7 C. C. Schreib, M. I. Jarvis, T. Terlier, J. Goell, S. Mukherjee, M. D. Doerfert, T. A. Wilson, M. Beauregard, K. N. Martins, J. Lee, L. D. S. Solis, E. Vazquez, M. A. Oberli, B. W. Hanak, M. Diehl, I. Hilton and O. Veiseh, *Adv. Mater.*, 2023, **35**, 2205709.
8 S. Bose, L. R. Volpatti, D. Thiono, V. Yesilyurt, C. McGladrigan, Y. Tang, A. Facklam, A. Wang, S. Jhunjhunwala, O. Veiseh, J. Hollister-Lock, C. Bhattacharya, G. C. Weir, D. L. Greiner, R. Langer and D. G. Anderson, *Nat. Biomed. Eng.*, 2020, **4**, 814–826.
9 X. Xie, J. C. Doloff, V. Yesilyurt, A. Sadraei, J. J. McGarrigle, M. Omami, O. Veiseh, S. Farah, D. Isa, S. Ghani, I. Joshi, A. Vegas, J. Li, W. Wang, A. Bader, H. H. Tam, J. Tao, H. J. Chen, B. Yang, K. A. Williamson, J. Oberholzer, R. Langer and D. G. Anderson, *Nat. Biomed. Eng.*, 2018, **2**, 894–906.
10 A. J. Vegas, O. Veiseh, J. C. Doloff, M. Ma, H. H. Tam, K. Bratlie, J. Li, A. R. Bader, E. Langan, K. Olejnik, P. Fenton, J. W. Kang, J. Hollister-Locke, M. A. Bochenek, A. Chiu, S. Siebert, K. Tang, S. Jhunjhunwala, S. Aresta-Dasilva, N. Dholakia, R. Thakrar, T. Vietti, M. Chen, J. Cohen, K. Siniakowicz, M. Qi, J. McGarrigle, A. C. Graham, S. Lyle, D. M. Harlan, D. L. Greiner, J. Oberholzer, G. C. Weir, R. Langer and D. G. Anderson, *Nat. Biotechnol.*, 2016, **34**, 345–352.
11 S. Mukherjee, B. Kim, L. Y. Cheng, M. D. Doerfert, J. Li, A. Hernandez, L. Liang, M. I. Jarvis, P. D. Rios, S. Ghani, I. Joshi, D. Isa, T. Ray, T. Terlier, C. Fell, P. Song, R. N. Miranda, J. Oberholzer, D. Y. Zhang and O. Veiseh, *Nat. Biomed. Eng.*, 2023, **7**, 867–886.
12 Q. Liu, A. Chiu, L. H. Wang, D. An, M. Zhong, A. M. Smink, B. J. de Haan, P. de Vos, K. Keane, A. Vegge, E. Y. Chen, W. Song, W. F. Liu, J. Flanders, C. Rescan, L. G. Grunnet, X. Wang and M. Ma, *Nat. Commun.*, 2019, **10**, 5262.
13 M. A. Bochenek, O. Veiseh, A. J. Vegas, J. J. McGarrigle, M. Qi, E. Marchese, M. Omami, J. C. Doloff, J. Mendoza-Elias, M. Nourmohammadzadeh, A. Khan, C. C. Yeh, Y. Xing, D. Isa, S. Ghani, J. Li, C. Landry, A. R. Bader, K. Olejnik, M. Chen, J. Hollister-Lock, Y. Wang, D. L. Greiner, G. C. Weir, B. L. Strand, A. M. A. Rokstad, I. Lacik, R. Langer, D. G. Anderson and J. Oberholzer, *Nat. Biomed. Eng.*, 2018, **2**, 810–821.
14 A. J. Vegas, O. Veiseh, M. Gurtler, J. R. Millman, F. W. Pagliuca, A. R. Bader, J. C. Doloff, J. Li, M. Chen, K. Olejnik, H. H. Tam, S. Jhunjhunwala, E. Langan, S. Aresta-Dasilva, S. Gandham, J. J. McGarrigle, M. A. Bochenek, J. Hollister-Lock, J. Oberholzer, D. L. Greiner, G. C. Weir, D. A. Melton, R. Langer and D. G. Anderson, *Nat. Med.*, 2016, **22**, 306–311.
15 H. Yan, C. Seignez, M. Hjorth, B. Winkeljann, M. Blakeley, O. Lieleg, M. Phillipson and T. Crouzier, *Adv. Funct. Mater.*, 2019, **29**, 1902581.

16 Q. Liu, X. Wang, A. Chiu, W. Liu, S. Fuchs, B. Wang, L. H. Wang, J. Flanders, Y. Zhang and K. Wang, *Adv. Mater.*, 2021, **33**, 2102852.
17 Q. Liu, X. Wang, A. Chiu, W. Liu, S. Fuchs, B. Wang, L. H. Wang, J. Flanders, Y. Zhang, K. Wang, J. M. Melero-Martin and M. Ma, *Adv. Mater.*, 2021, **33**, 2102852.
18 L.-H. Wang, A. U. Ernst, J. A. Flanders, W. Liu, X. Wang, A. K. Datta, B. Epel, M. Kotecha, K. K. Papas and M. Ma, *Sci. Adv.*, 2021, **7**, eabd5835.
19 R. Chang, J. L. Chen, G. Y. Zhang, Y. Li, H. Z. Duan, S. Z. Luo and Y. X. Chen, *J. Am. Chem. Soc.*, 2022, **144**, 12147–12157.
20 D. Zhang, Q. Chen, Y. Bi, H. Zhang, M. Chen, J. Wan, C. Shi, W. Zhang, J. Zhang and Z. Qiao, *Nat. Commun.*, 2021, **12**, 1–12.
21 D. Zhang, Q. Chen, W. Zhang, H. Liu, J. Wan, Y. Qian, B. Li, S. Tang, Y. Liu, S. Chen and R. Liu, *Angew. Chem., Int. Ed.*, 2020, **59**, 9586–9593.
22 S. Farah, J. C. Doloff, P. Muller, A. Sadraei, H. J. Han, K. Olafson, K. Vyas, H. H. Tam, J. Hollister-Lock, P. S. Kowalski, M. Griffin, A. Meng, M. McAvoy, A. C. Graham, J. McGarrigle, J. Oberholzer, G. C. Weir, D. L. Greiner, R. Langer and D. G. Anderson, *Nat. Mater.*, 2019, **18**, 892–904.
23 D. Dong, C. Tsao, H.-C. Hung, F. Yao, C. Tang, L. Niu, J. Ma, J. MacArthur, A. Sinclair and K. Wu, *Sci. Adv.*, 2021, **7**, eabc5442.
24 L. Zhang, Z. Cao, T. Bai, L. Carr, J. R. Ella-Menye, C. Irvin, B. D. Ratner and S. Jiang, *Nat. Biotechnol.*, 2013, **31**, 553–556.
25 J. T. Chung, C. M. L. Lau, C. H. Y. Chung, M. Rafiei, S. Yao and Y. Chau, *Biomater. Sci.*, 2023, **11**, 4827–4844.
26 Q. Li, C. Wen, J. Yang, X. Zhou, Y. Zhu, J. Zheng, G. Cheng, J. Bai, T. Xu, J. Ji, S. Jiang, L. Zhang and P. Zhang, *Chem. Rev.*, 2022, **122**, 17073–17154.
27 Y. K. Kim, E. Y. Chen and W. F. Liu, *J. Mater. Chem. B*, 2016, **4**, 1600–1609.
28 Z. Zhang, T. Chao, L. Liu, G. Cheng, B. D. Ratner and S. Jiang, *J. Biomater. Sci., Polym. Ed.*, 2009, **20**, 1845–1859.
29 L. E. Jansen, L. D. Amer, E. Y. T. Chen, T. V. Nguyen, L. S. Saleh, T. Emrick, W. F. Liu, S. J. Bryant and S. R. Peyton, *Biomacromolecules*, 2018, **19**, 2880–2888.
30 E. Zhang, Y. Shi, H. Han, H. Zhu, B. Song, C. Yang and Z. Cao, *Nat. Biomed. Eng.*, 2023, DOI: **10.1038/s41551-023-01108-z**.
31 M. T. Larsen, M. Kuhlmann, M. L. Hvam and K. A. Howard, *Mol. Cell. Ther.*, 2016, **4**, 1–12.
32 B. Elsadek and F. Kratz, *J. Controlled Release*, 2012, **157**, 4–28.
33 D. Sleep, *Expert Opin. Drug Delivery*, 2015, **12**, 793–812.
34 J. Ling, T. Huang, R. Wu, C. Ma, G. Lin, Z. Zhou, J. Wang, Q. Tu, X. Tang, Y. Liu, M. Liu, L. Yang and Y. Yang, *Adv. Funct. Mater.*, 2023, **33**, 2213342.
35 D. Zhang, Q. Chen, Y. Bi, H. Zhang, M. Chen, J. Wan, C. Shi, W. Zhang, J. Zhang, Z. Qiao, J. Li, S. Chen and R. Liu, *Nat. Commun.*, 2021, **12**, 5327.
36 X. Tang, X. Chen, S. Zhang, X. Gu, R. Wu, T. Huang, Z. Zhou, C. Sun, J. Ling, M. Liu and Y. Yang, *Adv. Funct. Mater.*, 2021, **31**, 2101320.
37 M. Li, G. Wu, M. Wang, E. B. Hunziker and Y. Liu, *Nanomaterials*, 2022, **12**, 2439.
38 C. Tao, W. Z. Zhu, J. Iqbal, C. J. Xu and D. A. Wang, *J. Mater. Chem. B*, 2020, **8**, 6080–6091.
39 A. M. Merlot, D. S. Kalinowski and D. R. Richardson, *Front. Physiol.*, 2014, **5**, 299.
40 M. T. Larsen, M. Kuhlmann, M. L. Hvam and K. A. Howard, *Mol. Cell. Ther.*, 2016, **4**, 3.
41 B. Elsadek and F. Kratz, *J. Controlled Release*, 2012, **157**, 4–28.
42 F. F. An and X. H. Zhang, *Theranostics*, 2017, **7**, 3667–3689.
43 Z. Zhang, H. Vaisocherová, G. Cheng, W. Yang, H. Xue and S. Jiang, *Biomacromolecules*, 2008, **9**, 2686–2692.
44 A. S. A. Habeeb, *Anal. Biochem.*, 1966, **14**, 328–336.
45 N. Noskovicova, R. Schuster, S. van Putten, M. Ezzo, A. Koehler, S. Boo, N. M. Coelho, D. Griggs, P. Ruminski, C. A. McCulloch and B. Hinz, *Nat. Biomed. Eng.*, 2021, **5**, 1437–1456.
46 R. A. Scott, K. L. Kiick and R. E. Akins, *Acta Biomater.*, 2021, **122**, 220–235.
47 A. K. Blakney, M. D. Swartzlander and S. J. Bryant, *J. Biomed. Mater. Res., Part A*, 2012, **100A**, 1375–1386.
48 L. Mi and S. Jiang, *Angew. Chem., Int. Ed.*, 2014, **53**, 1746–1754.
49 J. Ong, J. Zhao, A. W. Justin and A. E. Markaki, *Biotechnol. Bioeng.*, 2019, **116**, 3457–3468.
50 J. C. Doloff, O. Veiseh, A. J. Vegas, H. H. Tam, S. Farah, M. Ma, J. Li, A. Bader, A. Chiu, A. Sadraei, S. Aresta-Dasilva, M. Griffin, S. Jhunjhunwala, M. Webber, S. Siebert, K. Tang, M. Chen, E. Langan, N. Dholokia, R. Thakrar, M. Qi, J. Oberholzer, D. L. Greiner, R. Langer and D. G. Anderson, *Nat. Mater.*, 2017, **16**, 671–680.